ISSN (Print) 1226-1750
ISSN (Online) 2233-6656
Journal of Magnetics 19(4), 393-398 (2014) http://dx.doi.org/10.4283/JMAG.2014.19.4.393

Design of Coaxial Magnetic Gear for Improvement of Torque Characteristics

H. M. Shin and J. H. Chang*

Electrical Engineering Department, Dong-A University, Saha-gu, Busan 604-714, Korea

(Received 1 August 2014, Received in final form 25 September 2014, Accepted 25 September 2014)

This paper proposes new types of models that have coaxial magnetic gear (CMG) configurations to increase torque transmission capability. They have flux concentrating structures at the outer low speed rotor, and permanent magnets (PMs) are embedded in the space between stationary pole pieces. The torque performances of the proposed models are compared with those of a basic CMG model. The harmonic torque components due to air gap field harmonics are also analyzed to investigate the torque contribution of each harmonic by using finite element analysis (FEA) and the Maxwell stress tensor. The proposed CMG model is optimized to have high torque density with low torque ripples by response surface methodology (RSM). Compared to the basic CMG model, the proposed model has a huge increase in transmitted torque density, and is very advantageous in term of PM use.

Keywords : coaxial magnetic gear, flux concentrating structure, magnetic gearing effect, torque characteristics

1. Introduction

The magnetic gear has many advantages, including low vibration, minimum acoustic noise, maintenance free operation, and inherent overload protection. This is caused by the contactless structure of the magnetic gear with physical isolation between the input and output shafts. Despite these benefits, the magnetic gear's use in industrial applications has been limited owing to its low torque transmission capability, compared to mechanical gears. To overcome the poor torque density of the magnetic gear, a coaxial magnetic gear (CMG) with surface-mounted permanent magnets (PMs) was introduced [1, 2], and many variants of the CMG have been proposed, with different configurations of PMs [3-7].

In 2009, Liu proposed a new topology for the concentric magnetic gear. The PMs in the outer rotor are inserted into the iron core. Thus, the PM material can be saved while the torque density is maintained [4]. Jian proposed a Halbach array in the configuration of the inner and outer rotor PMs. This would produce sinusoidal magnetic field distribution at the air gap region and improve torque transmission [5]. In 2011, Li adopted a spoke-type structure on the outer rotor to concentrate magnetic flux [6]. Another model that uses the flux focusing effect, introduced in 2013, has the PMs inserted between stationary pole pieces and magnetized in a circumferential direction [7]. The inner rotor of it has a salient-pole surface-mounted PM configuration, and the outer rotor employs a simple tooth-slot structure without PMs to increase the torque per unit PM volume. However, these variants of CMG models still could not achieve comparable performance in torque density with their mechanical counterparts.

This paper proposes new models of CMG configurations. They have flux concentrating structures at the outer low speed rotor, and the PMs are magnetized in a radial direction and inserted between stationary pole pieces. The torque characteristics of the proposed models are compared with those of the basic CMG model in terms of torque density, torque ripples, and generated torque per unit PM volume. Harmonic torque components due to air gap field harmonics are also analyzed to investigate the torque contribution of each harmonic by using finite element analysis (FEA) and the Maxwell stress tensor [8, 9]. Finally, response surface methodology (RSM) is used to maximize the torque with low torque ripples. The analysis results show that the proposed models have a huge increase in torque density and in the generated torque per unit PM volume, compared to the basic CMG model.

*Corresponding author: Tel: +82-51-200-7735
Fax: +82-51-200-7743, e-mail: cjhwan@dau.ac.kr

2. Comparison of Torque Characteristics

2.1. Analytical Model

Fig. 1 shows the structure of a basic CMG. It consists of two counter rotating parts, an inner high speed rotor and outer low speed rotor, and stationary pole pieces. The magnetic flux produced by the PMs is modulated by the ferromagnetic pole pieces. The dominant harmonics of it are corresponded to the number of pole pairs of each rotor to generate a magnetic gearing effect. The analysis model has 4 pole pairs in the high speed rotor and 22 pole pairs in the low speed rotor, resulting in a gear ratio of 5.5:1. The other important parameters are shown in Table 1.

In the proposed models, the PMs mounted on the outer rotor are replaced with PMs that have a flux concentrating structure, as shown in Fig. 2(a). The magnetic flux produced by the flux concentrating structure flows in a radially inward direction, and the extruding teeth play a role as opposite poles. With this structure, the magnetic flux density of the air gap region can be increased. In addition, the stiffness of the outer rotor can be improved, and the PM material can be saved. Another proposed variant in the CMG configuration has the PMs embedded in the space between the ferromagnetic pole pieces, as shown in Fig. 2(b). These added PMs are magnetized in the same direction and are used to increase the air gap flux density and torque transmission capabilities

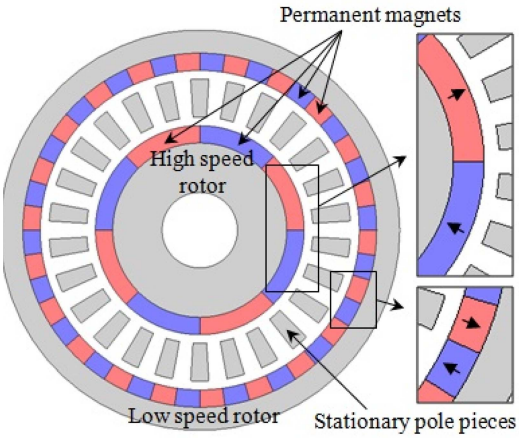

Fig. 1. (Color online) Basic CMG model.

Table 1. Specifications of the analysis model.

Parameters	Value
Number of pole pairs on inner rotor	4
Number of pole pairs on outer rotor	22
Number of stationary pole pieces	26
Outer diameter [mm]	117
PM radial thickness [mm]	6
Remanence of PM [T]	1.25
Air gap thickness [mm]	1
Axial length [mm]	30

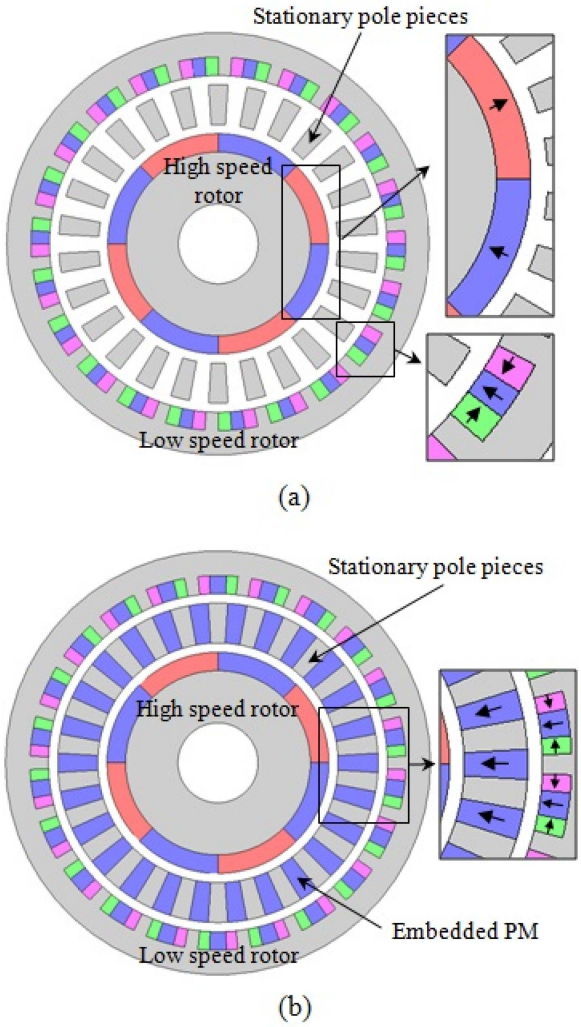

Fig. 2. (Color online) Proposed models having a CMG configuration: (a) proposed model I, (b) proposed model II.

2.2. Torque calculation

The electromagnetic torque calculation by the Maxwell stress tensor can be expressed in cylindrical coordinates using the radial and tangential flux densities around the air gap circumference, B_r and B_θ, respectively.

$$T(t) = \frac{r^2}{\mu_0}\int_0^{l_a}\int_0^{2\pi} B_r(\theta,t)B_\theta(\theta,t)d\theta dz \quad (1)$$

where l_a is the axial length, and r is the distance from the center of the rotor to the air gap for measuring the flux density. At each time, space distributions of the radial and tangential flux density can be harmonically decomposed as

$$B_r(\theta) = 2\sum_{v=1}^{\infty} |B_r^v| \cos(v\theta + \hat{\phi}_v) \quad (2)$$

$$B_\theta(\theta) = 2\sum_{w=1}^{\infty} |B_\theta^w| \cos(w\theta + \hat{\phi}_w) \quad (3)$$

where v and w are harmonic orders, and $\hat{\phi}_v$ and $\hat{\phi}_w$ are the harmonic phases corresponding to each harmonic in the radial and tangential flux distributions, respectively. The electromagnetic torque at each time is derived by substitution of (2) and (3) into (1). The resultant harmonic torque equation can be expressed using the phase angle between the m^{th} harmonic of the radial and tangential field, ϕ_{ph}^m [9].

$$T(\theta) = \frac{4\pi l_a r^2}{\mu_0} \sum_{m=1}^{\infty} |B_r^m||B_\theta^m| \cos(\phi_{ph}^m) \quad (4)$$

2.3. Flux density and harmonic component

Fig. 3 shows the radial flux density distribution and the corresponding space harmonic spectrum of the basic model and proposed model I in the air gap adjacent to the low speed rotor. In proposed model I, the harmonic components corresponding with the number of pole pairs of both rotors are increased owing to the flux focusing effect. Similarly, Fig. 4 shows the radial flux density distribution and corresponding space harmonic spectrum of the basic model and proposed model II in the air gap adjacent to the low speed rotor. It also has an increase in the harmonics of 4 and 22 orders corresponding to the number of rotor pole pairs. Compared to proposed model I, there is a remarkable increase in the 26th harmonic, which is caused by the PMs embedded between the stationary pole pieces.

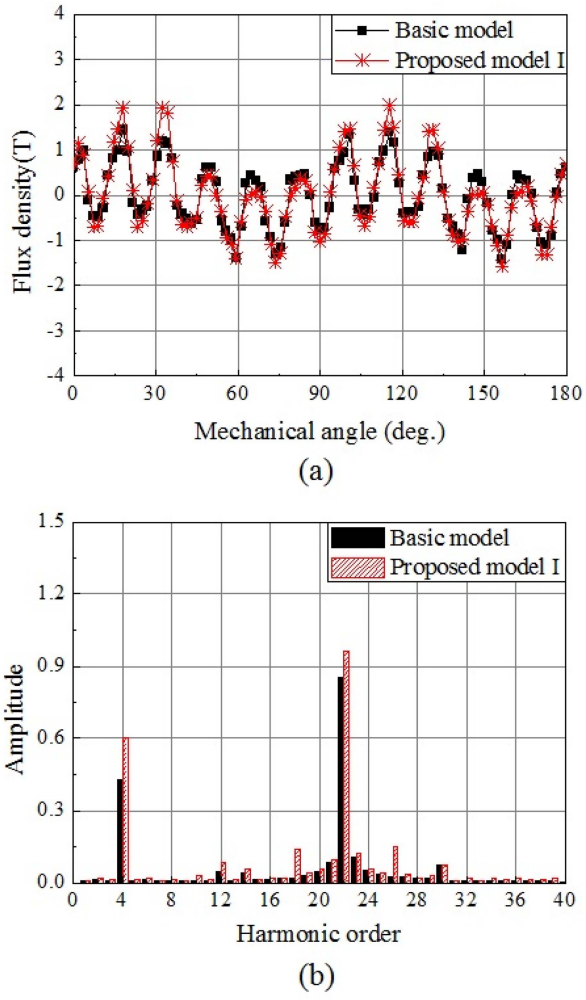

Fig. 3. (Color online) Radial flux of the basic model and proposed model I in the outer air gap: (a) magnetic flux density distribution, (b) space harmonic spectrum.

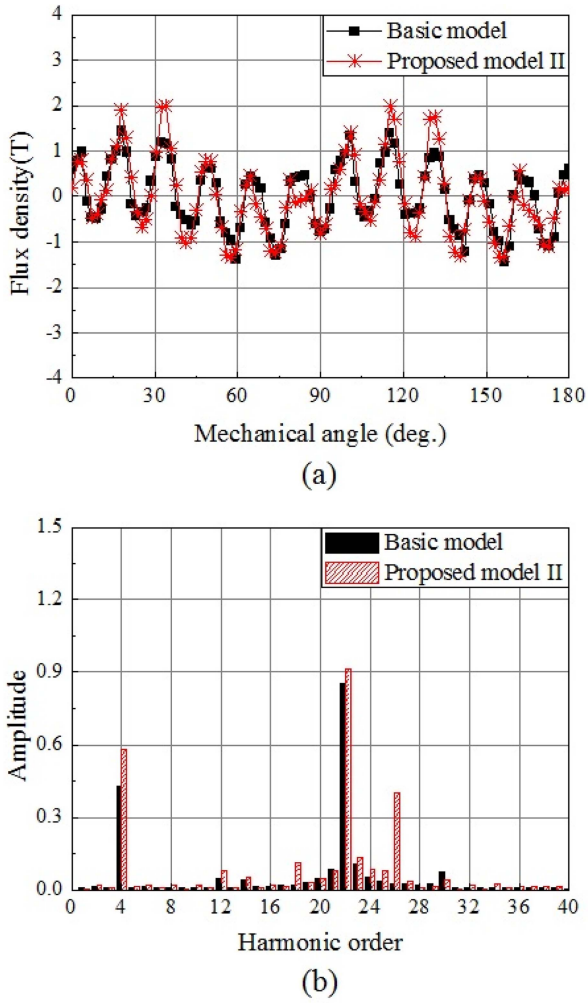

Fig. 4. (Color online) Radial flux of the basic model and proposed model II in the outer air gap: (a) magnetic flux density distribution, (b) space harmonic spectrum.

Table 2. Harmonic torque contribution.

Harmonic	Basic model		Proposed model I		Proposed model II	
Order	Inner rotor	Outer rotor	Inner rotor	Outer rotor	Inner rotor	Outer rotor
4	6.03	0.02	6.55	0.20	7.69	1.95
12	0.01	0.01	0.01	0.07	0.25	0.11
20	0.03	·	·	·	0.06	·
22	0.01	32.82	·	34.00	0.01	32.80
26	·	·	·	0.15	0.09	11.50
28	0.05	·	0.05	·	0.05	0.01
30	·	0.03	0.01	0.11	·	0.05
34	·	·		0.04	·	0.06
36	0.02	·	0.02	·	0.02	·
40	·	·	·	0.13	·	0.10
44	0.01	·	0.01	0.15	0.01	0.10
48	·	0.02	·	2.50	·	2.12
52	0.01	0.01	·	0.04	0.50	0.10
Total Harmonic Torque	6.14	33.41	6.66	36.05	8.22	44.43
Virtual Work Method	6.09	33.48	6.59	36.25	8.13	44.60

2.4. Torque contribution by harmonic component

Table 2 shows the torque contribution of each harmonic component of the magnetic flux density. The superposition of harmonic torque components agrees with the results of the virtual work method based on the FEA. The harmonics corresponding to the number of pole pairs of each rotor have a great effect on torque transmission. In proposed model I, the magnitudes of the harmonic components of the 4th and 22nd orders are increased owing to the flux concentrating structure, and they have a dominant effect on the increase in the total generated torque. In proposed model II, the 26th harmonic component has a big influence on the developed torque, unlike in proposed model I. This results in an increase in the transmitted torque. By contrast, the torque contribution of the 22nd harmonic component of proposed model II is smaller than that of proposed model I, even though the magnitude of multiplication of each corresponding harmonic component is almost the same. This is due to the fact that the harmonic torque equation has a cosine function term of phase angle between the radial and tangential field harmonics. A similar situation occurs when only embedded PMs are employed in the basic CMG model. Although it also has 26th harmonic components in the air gap field like the proposed model II, it does not have harmonic torque produced by them because they have almost a 90^{o} phase difference. Instead, the generated torque is decreased by a reduction in the main harmonics.

In contrast with the increase in transmitted torque, proposed model II has significant torque ripples in the force profile of the high speed rotor as shown in Fig. 5. Based on the harmonic torque analysis, it is inferred that this is mainly due to the 52nd air gap harmonic fields and should be minimized.

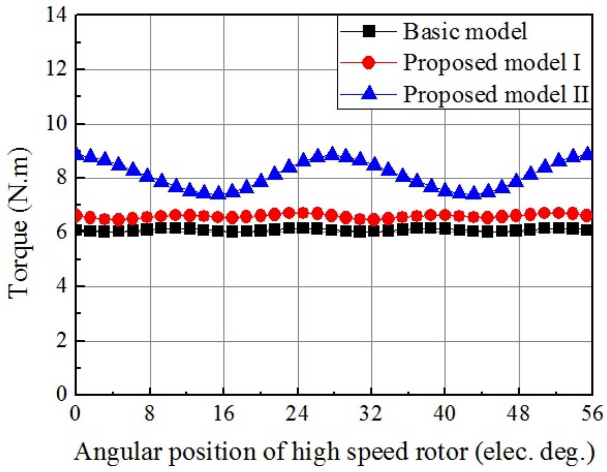

Fig. 5. (Color online) Variation in torque in the high speed rotor with angular position.

3. Parameters Optimization

The design of proposed model II is optimized using RSM to improve its torque characteristics [10-12]. RSM is a statistical optimization method that could be well adapted to develop an analytical model for complex problems in which a response of interest is influenced by

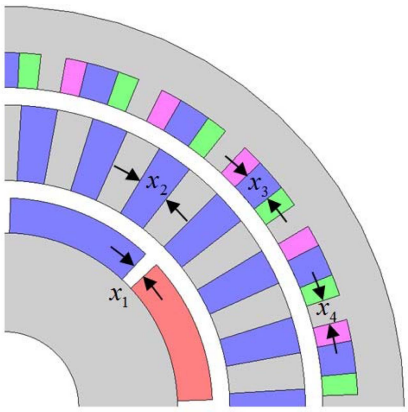

Fig. 6. (Color online) Design variables for optimization.

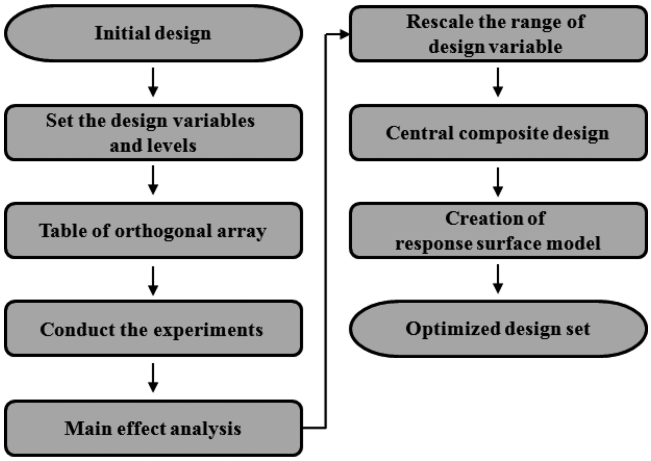

Fig. 7. Flow chart of optimum design.

several variables. The design goal is to maximize the transmitted torque with reduced torque ripples. As first step, the most influential design variables are selected, as shown in Fig. 6. The values of each design variable are in proportion to the reference values. S1 is the ratio of the non magnetized area (x_1) with respect to the pole pitch of the high speed rotor, S2 is the width ratio between the inserted PM (x_2) and the stationary pole piece, S3 is the length ratio in the circumferential direction between the radially magnetized PM (x_3) and tangentially magnetized PM, and S4 is the ratio of the tooth width (x_4) to one third of PM width on the outer rotor. Fig. 7 shows a flow chart describing the optimization process using RSM. At first step, design variables are selected and their levels are arranged in the table of orthogonal array. The torque characteristics on each experiment are analyzed by FEA. Main effect analysis using ANOM (analysis of mean) is used to determine the most influencing design variables and their range. Based on these results, design variables

Table 3. Optimized design set.

Location	Parameter	Optimum value
High speed rotor	S1	0.1
Stationary ring	S2	1
Low speed rotor	S3	1.5
	S4	1

Table 4. Comparison of torque characteristics between models.

Content		Basic model	Proposed model I	Proposed model II	Proposed model III
Torque (N.m)	Inner rotor	6.09 (100%)	6.79 (112%)	8.17 (134%)	7.55 (124%)
	Outer rotor	33.48 (100%)	37.33 (112%)	44.94 (134%)	41.54 (124%)
Ripple (%)	Inner rotor	2.14	3.18	3.00	1.57
	Outer rotor	0.04	0.15	0.64	0.39
Torque/volume ($kN.m/m^3$)		103.8 (100%)	115.7 (112%)	139.3 (134%)	128.8 (124%)
Torque/PM ($kN.m/m^3$)		340.2 (100%)	465.8 (137%)	465.4 (137%)	470.2 (138%)

are rescaled and arranged by central composite design. After the designed experiment is performed, with the use of RSM, an approximated equation representing response surface of the torque characteristics can be obtained. Finally, the most desired design set is selected as shown in Table 3.

With these optimized design values, the torque characteristics of the CMG models are compared in Table 4. Proposed model I has an increment of 12% in the pull-out torque compared to the basic model. This model can produce 37% more torque than the basic model with the same volume of PM. Proposed model II produces the biggest torque and the torque per unit PM volume also has increased by 37% compare to the basic model. It has comparable torque ripples to the other models with optimized design variables. In contrast to the increased torque, proposed model II has similar torque per unit PM volume as the proposed model I. This is because of the PM inserted between the stationary pole pieces. To observe the influence of the inserted PM, the variations in torque characteristics are analyzed depending on the length ratio in the radial direction between the inserted PM and stationary pole piece, as shown in Fig. 8. Proposed models I and II correspond to the embedded PM ratios of 0 and 1, respectively. While the torque of proposed model II is linearly increased as the ratio of embedded PM is getting closer to one, there is little change

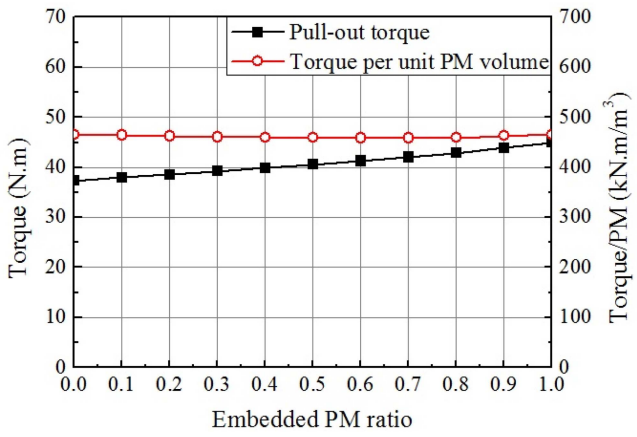

Fig. 8. (Color online) Pull-out torque and torque density per unit PM volume of the low speed rotor.

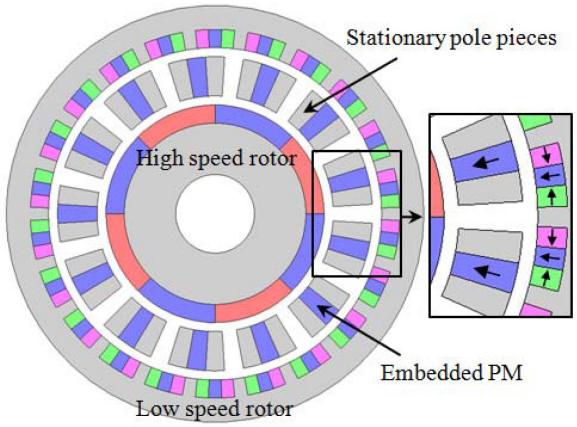

Fig. 9. (Color online) Proposed model III.

in the torque per unit PM volume. There is another variant, proposed model III, of the CMG model, as shown in Fig. 9. It has the same structure as proposed model II, except that the PMs are inserted in every other space in the stationary pole pieces. The pull-out torque of proposed model III is reduced compared to that of proposed model II. But it can save the PM materials and increase the torque per unit PM volume.

4. Conclusion

This paper proposes new types of CMG models that have a flux concentrating structure in the outer low speed rotor and embedded PMs in the space between stationary pole pieces. The proposed models have an increment in the torque density up to 34% compared to the basic CMG model. The analysis results also show that the proposed models can increase their transmitted torque per unit PM volume up to 38% depending on the PM arrangement.

Acknowledgment

This research was supported by Basic Science Research Program through the National Research Foundation of Korea (NRF) funded by the Ministry of Education, Science and Technology (NRF-2012R1A1A2044307) and Human Resources Development program (No. 20134030200320) of the Korea Institute of Energy Technology Evaluation and Planning (KETEP) grant funded by the Korea government Ministry of Trade, Industry and Energy.

References

[1] K. Atallah and D. Howe, IEEE Trans. Magn. **37**, 2844 (2001).
[2] K. Atallah, S. D. Calverley, and D. Howe, IEE Proc-Electr. Power Appl. **151**, 135 (2004).
[3] P. O. Rasmussen, T. O. Andersen, F. T. Jorgensen, and O. Nielsen, IEEE Trans. Ind. Appl. **41**, 764 (2005).
[4] X. Liu, K. T. Chau, J. Z. Jiang, and C. Yu, J. Appl. Phys. **105**, 07F101 (2009).
[5] L. Jian and K. T. Chau, IEEE Trans. Energy Convers. **25**, 319 (2010).
[6] X. Li, K. T. Chau, M. Cheng, W. Hua, and Y. Du, Proceedings of the International Conference on Electrical Machine and Systems (ICEMS) (2011) pp. 1-4.
[7] Xianglin Li, K. T. Chau, Ming Cheng, Wei Hua, and Yi Du, Proceedings of the International Conference on Electrical Machine and Systems (ICEMS) (2013) pp. 634-638.
[8] K. J. Meessen, J. J. H. Paulides, and E. A. Lomonova, IEEE Trans. Magn. **49**, 536 (2013).
[9] C. M. Spargo, B. C. Mecrow, and J. D. Widmer, IEEE Trans. Magn. **50**, 1 (2014).
[10] X. K. Gao, T. S. Low, S. X. Chen, and Z. J. Liu, IEEE Trans. Magn. **37**, 2814 (2001).
[11] J. T. Li, Z. J. Liu, M. A. Jabbar, and X. K. Gao, IEEE Trans. Magn. **40**, 1176 (2004).
[12] R. H. Myers, D. C. Montgomery, and C. M. Anderson-Cook, Response Surface Methodology (2008).